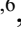
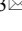
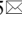
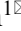


AutoMAT: A Hierarchical Framework for Autonomous Alloy Discovery

Penghui Yang^{1,6}, Chendong Zhao^{2,6}, Bijun Tang², Zhonghan Zhang¹, Xinrun Wang³,
Yanchen Deng¹, Yuhao Lu¹, Cuntai Guan¹, Zheng Liu^{2,4,5}, Bo An¹

¹College of Computing and Data Science, Nanyang Technological University, Singapore 639798, Singapore

²School of Materials Science and Engineering, Nanyang Technological University, Singapore 639798, Singapore

³School of Computing and Information Systems, Singapore Management University, Singapore 188065

⁴CINTRA CNRS/NTU/THALES, UMI 3288, Research Techno Plaza, 50 Nanyang Drive, Border X Block, Level 6, Singapore 637553, Singapore

⁵Institute for Functional Intelligent Materials, National University of Singapore, Singapore, Singapore

⁶These authors contributed equally: Penghui Yang, Chendong Zhao

E-mail: bjtang@ntu.edu.sg; xrwang@smu.edu.sg; z.liu@ntu.edu.sg; boan@ntu.edu.sg

Alloy discovery is central to advancing modern industry but remains hindered by the vastness of compositional design space and the costly validation. Here, we present AutoMAT, a hierarchical and autonomous framework grounded in and validated by experiments, which integrates large language models, automated CALPHAD-based simulations, and AI-driven search to accelerate alloy design. Spanning the entire pipeline from ideation to validation, AutoMAT achieves high efficiency, accuracy, and interpretability without the need for manually curated large datasets. In a case study targeting a lightweight, high-strength alloy, AutoMAT identifies a titanium alloy with 8.1% lower density and comparable yield strength relative to the state-of-the-art reference, achieving the highest specific strength among all comparisons. In a second case targeting high-yield-strength high-entropy alloys, AutoMAT achieves a 28.2% improvement in yield strength over the base alloy. In both cases, AutoMAT reduces the discovery timeline from years to weeks, illustrating its potential as a scalable and versatile platform for next-generation alloy design.

Introduction

Alloy design underpins the development of advanced structural materials across aerospace, automotive, and biomedical sectors^{1,2}. Historically, alloy discovery has been guided by systems centered around one principal element, gradually evolving toward more complex compositions to meet rising performance demands, such as high-strength steels^{3,4}. Yet even with a modest number of alloying elements, the compositional design space expands combinatorially, yielding up to 10^{50} possible combinations⁵⁻⁷. Exhaustive experimental exploration of this high-dimensional space is infeasible, rendering traditional trial-and-error approaches fundamentally unsuitable for modern materials design challenges⁸.

Computational methods have been developed to address this issue, but most still require trade-offs between speed, accuracy, generalizability, and cost. Machine learning (ML)-based approaches can rapidly screen candidates, but often suffer from poor data efficiency, limited interpretability, and restricted generalization to new material systems⁹⁻¹¹. Large language models (LLMs) offer new opportunities for knowledge retrieval, yet cannot directly predict physical properties¹². Conversely, physics-based simulations such as CALPHAD and density functional theory (DFT) deliver accurate and interpretable results, but are computationally expensive and typically require substantial manual effort¹³⁻¹⁵. A holistic solution that combines automation, data efficiency, physical fidelity, and scalability remains elusive.

Here, we introduce AutoMAT, a hierarchical and autonomous framework for alloy discovery that integrates LLMs, automated CALPHAD simulations, AI-driven search, and experimental validation. To our knowledge, AutoMAT is the first system to autonomously span the entire alloy design pipeline, from ideation and simulation to experimental validation, marking a step toward more sustainable, interpretable, and scalable materials innovation^{16,17}. The framework is structured into three tiers, each addressing a distinct stage of the design process. The Ideation Layer leverages LLMs to extract, process, and propose candidate alloy systems from scientific literature and handbooks based on user-defined property targets (e.g., high yield strength, low density, etc.), outputting structured suggestions (e.g., JSON) within minutes. These are refined in the Simulation Layer, where CALPHAD-based thermodynamic modeling is fully automated for the first time and coupled with AI-guided search. This dramatically reduces the number of required evaluations from up to hundreds of thousands to just a few thousand, while balancing predictive accuracy and computational efficiency with minimal human input. The final Validation Layer performs experimental synthesis and

characterization of top-ranked candidates. While inherently slower, it provides critical verification, ensuring that computationally optimized alloys deliver the desired properties. As illustrated in Fig. 1a, AutoMAT integrates the complementary strengths of each method: LLMs for intelligent and data-efficient knowledge integration; CALPHAD for thermodynamic accuracy and interpretability; AI-driven search for high-throughput time efficiency and automation. Detailed rating criteria and justifications for the method comparisons are provided in Supplementary Note 1. Overall, AutoMAT offers unprecedented generalizability and experimental efficiency for alloy design.

In alloy design, composition plays a primary role in determining baseline mechanical properties, which can later be tailored through deformation or annealing. This study focuses on as-cast alloys—produced via arc melting and solidified without post-processing—as they reflect the intrinsic mechanical response governed by composition, solid solution strengthening, and grain boundary effects. These unprocessed states serve as a consistent basis for evaluating and optimizing alloy performance. These unprocessed states provide a basis for alloy evaluation and optimization. To demonstrate the effectiveness and generalizability of the AutoMAT framework, we present two case studies with distinct design goals: the first targets a bulk lightweight alloy with excellent mechanical performance to show its capability of addressing multi-objective optimization¹⁵; the second showcases its feasibility in a vastly larger design space by identifying a low-cost high-entropy alloy (HEA) with high yield strength for potential structural applications. These examples illustrate how the hierarchical integration of literature-informed ideation, physics-based simulation, and experimental validation can accelerate alloy discovery while minimizing dependence on expert intervention.

Results

System Overview

We developed a hierarchical, three-tier system to enable autonomous and scalable discovery of alloys, integrating LLMs, advanced AI-driven search algorithms, CALPHAD-based simulations, and experimental validation (Fig. 1). The system translates user-defined property targets into physically validated alloy compositions, operating with minimal human input. Each layer plays a distinct role in this end-to-end discovery pipeline: LLM-driven ideation, simulation-based refinement, and experimental confirmation.

The Ideation Layer initiates the process by leveraging LLMs (e.g., ChatGPT and Claude) to propose candidate alloy systems aligned with user-defined property requirements, such as

high yield strength, low density, or cost constraints. The first task is alloy system selection. The LLM evaluates which alloy system can satisfy the specific criteria; if none, it recommends the alloy system satisfy the requirements as much as possible, thereby narrowing the design space. Once the appropriate system is identified, the LLM extracts candidate compositions from relevant literature, with a preference for alloy handbooks over review articles. Handbooks are priorities because they contain structured, text-based data that is easier for the LLM to parse, whereas reviews often present data in figures or tables, making extraction more difficult. This step outputs scientifically grounded, structured composition suggestions within minutes, providing an efficient and flexible entry point into the autonomous discovery workflow.

A cornerstone of our methodology is the Simulation Layer, which, for the first time, fully and automatically integrates CALPHAD thermodynamic calculations into a closed-loop material discovery process. This breakthrough is achieved through a dedicated API that transforms CALPHAD from a traditional, manually operated analysis tool into a dynamic, on-the-fly component of the autonomous optimization loop. The Simulation Layer systematically refines the LLM-generated candidates through an AI-driven iterative neighborhood search. This layer explores locally optimal compositions by adjusting elemental ratios around the initial candidates, first with coarse-grained steps to rapidly approach feasible regions, then narrowing to finer refinements once promising areas are identified: $x_{t+1} = \arg \max_{x' \in \mathcal{N}(x_t)} f(x')$, where $\mathcal{N}(x) = \{x' | x' \text{ is a neighbor of } x\}$. CALPHAD serves as the backbone of this process, offering precise and interpretable thermodynamic predictions. After acquiring the value of phase volume fractions by Scheil solidification¹⁸, the yield strength can be evaluated precisely and the reliability of the prediction was enhanced compared to AI models which can only predict yield strength directly from component information (Supplementary Fig. 1)¹⁹. These thermodynamic predictions are then used to guide each iteration toward meeting user-defined objectives. To maximize efficiency, the simulations are parallelized, enabling the evaluation of thousands of compositions per day, vastly outpacing traditional expert-driven CALPHAD workflows. Because a few additional iterations in this layer add little time compared to the Validation Layer, the search continues until reaching the maximum number of iterations, set at 5, to find a better component even if the requirements have already been met. Several assumptions are introduced to support full automation: grain size is fixed at 100 μm , which is the default grain size in the software; only consider intrinsic strength for the pure elements, grain boundary strength, and solid solution strengthening for composition-to-property prediction for materials design²⁰; and phases comprising less than 2% of volume

fraction are excluded as computational noise. These standardizations minimize human intervention while maintaining relevance and consistency. By combining the robust predictive power of CALPHAD with the efficiency of AI-driven search, the Simulation Layer delivers high-confidence alloy candidates, streamlining their transition to experimental validation.

The Validation Layer serves as the final stage of the platform, verifying computational predictions through experimental synthesis and characterization. Although this step operates on a longer timescale, typically requiring several weeks, it provides the essential ground truth to assess whether the proposed alloys meet real-world performance requirements. Key properties such as yield strength, density, and microstructural stability are measured to confirm the practical viability of each composition. Importantly, results from this layer can be looped back to earlier stages to refine search heuristics and improve the LLM's future recommendations, establishing a closed-loop system for continuous learning and iterative improvement.

By integrating the Ideation, Simulation, and Validation Layers into a cohesive, hierarchical workflow, the platform efficiently translates high-level user requirements into physically validated material solutions with minimal human intervention. Through the combination of rapid candidate generation, automated computational refinement, and experimental confirmation, it enables high-throughput, autonomous discovery of novel alloy compositions tailored to diverse performance objectives.

Case Study: Design of a Low-Density, High-Strength Alloys

To demonstrate the adaptability and effectiveness of our autonomous framework, we present a case study targeting a low-density, high-strength alloy. The target requirements included a yield strength approaching 850 MPa and a density below 4.36 g/cm³, with the goal of outperforming the state-of-the-art lightweight alloy Ti_{75.25}Al₂₀Cr_{4.75}²¹. Additional constraints included the use of at least four elements and the exclusion of high-cost elements. This complex, multi-objective design task illustrates AutoMAT's ability to make informed decisions across alloy families, optimize within large compositional space, and deliver experimentally validated solutions.

Literature-Guided Alloy Family Selection and Candidate Generation. The process began in the Ideation Layer with alloy system identification. In this step, the user-defined targets were translated into a prompt and passed to the LLM to evaluate which alloy system could meet both the high yield strength and low-density requirements. Recognizing it as a lightweight and high-strength alloy, the LLM recommended titanium alloys with comparable density and superior

strength based on its prior knowledge. This early assessment helped avoid unproductive computational exploration in an unsuitable design space. With titanium alloys selected, the Ideation Layer proceeded to handbook-guided candidate selection (Fig. 2b), where the system accessed a relevant titanium alloy handbook²².

The LLM was instructed to identify candidate alloys with at least four elements, consistent with multi-principal element design principles, while filtering out compositions containing prohibitively expensive elements. It then processed potential candidates through requirements verification (Fig. 2c) and component filtering (Fig. 2d). By parsing textual descriptions, the LLM extracted detailed data on mechanical properties and compositions. Among the qualified candidates, the LLM finally selected Ti86-Al1-V8-Fe5 (wt.%), corresponding to Ti81.4-Al16.8-V1.6-Fe0.2 (at%)—hereafter termed Ti-185—as the most suitable starting point. This alloy is known for its high yield strength with low density and is well-documented in the literature accessible via the handbook²². However, its estimated density (4.70 g/cm³) still exceeded the design target (< 4.36 g/cm³), necessitating further refinement in the Simulation layer.

The efficiency of this phase was notable. Leveraging the GPT-4o API, the LLM completed the alloy system identification, analyzed the handbook, and suggested Ti-185 as the viable candidate, all within minutes and at a computational cost of less than US\$1. In contrast, a thorough manual literature search would require several hours or even days. This efficiency highlights LLM's ability to provide a systematic and time-effective starting point for downstream exploration. Detailed prompts and LLM responses are provided in Supplementary Note 2.

Compositional Refinement through AI-Guided CALPHAD Optimization. Following the Ideation Layer, the initial candidate, Ti-185, was passed to the Simulation Layer for further optimization. Given the candidate's relatively high density, the primary objective was to reduce density while maintaining a high yield strength approaching 850 MPa. The Simulation Layer initiated its autonomous pipeline by leveraging CALPHAD-based methodologies for precise thermodynamic and physical property predictions. Its core strategy was an AI-driven iterative neighborhood search, which efficiently explored the compositional space, initially around Ti-185 and subsequently around the best compositions identified in each iteration.

The AI-driven search generated compositional variations by perturbing the current composition, using mole fraction differences to define distances between candidates. The

adaptivity of the search strategy was especially crucial here for two reasons. First, there was a significant mismatch between the initial candidate's high density and the desired target range, necessitating aggressive exploration. Second, the candidate's very low aluminum content constrained early compositional changes primarily to increasing the aluminum fraction. This limitation created a sparsely populated region in the compositional space where larger perturbations were both necessary and feasible, justifying the use of coarser step sizes in the initial search phase. Because the system needs to balance two competing objectives, i.e., maximizing yield strength while minimizing density, it becomes challenging to directly compare candidate compositions. To address this, we introduced a score function based on the specific strength, which serves as a single-objective proxy to guide the search. Specifically, we defined a score function as $f = \frac{\text{yield strength (MPa)}}{e^{\text{density (g/cm}^3\text{)}}}$, as shown in Fig. 3b. The exponential function of density was empirically chosen to strongly penalize heavier compositions, thereby biasing the search toward alloys with lower density while preserving mechanical strength.

Accordingly, the search began with a coarse-grained approach, employing a step size of 0.5 and a compositional search range of ± 10 mol%, with a focus on increasing aluminum content to rapidly shift toward lower-density regions. In this stage, the system identified Ti86.0-Al10.0-V3.5-Fe0.5, which achieved a substantial density reduction relative to the initial low-Al candidate while preserving high strength. Once promising candidates were identified, the algorithm transitioned to a fine-tuning mode using smaller step sizes of 0.2 and a narrowed search range of ± 2 mol% for local optimization around the best-performing compositions. All the search steps are shown below:

- Step 1: Ti86.0-Al10.0-V3.5-Fe0.5 $\rightarrow \rho = 4.460 \text{ g/cm}^3$, YS = 961.42 MPa, score = 11.116.
- Step 2: Ti84.2-Al11.8-V3.8-Fe0.2 $\rightarrow \rho = 4.437 \text{ g/cm}^3$, YS = 952.37 MPa, score = 11.268.
- Step 3: Ti82.8-Al13.0-V4.0-Fe0.2 $\rightarrow \rho = 4.427 \text{ g/cm}^3$, YS = 944.88 MPa, score = 11.292.
- Step 4: Ti82.2-Al15.0-V2.6-Fe0.2 $\rightarrow \rho = 4.387 \text{ g/cm}^3$, YS = 935.35 MPa, score = 11.634.
- Final step: Ti81.4-Al16.8-V1.6-Fe0.2 $\rightarrow \rho = 4.355 \text{ g/cm}^3$, YS = 927.08 MPa, score = 11.906.

Over the course of five refinement iterations, the simulation stopped on a composition that balanced both objectives. Although all the requirements are satisfied on Step 1, we still let the system to further optimize towards a better solution until the maximum iteration number is achieved. With multi-threaded execution, AutoMAT's Simulation Layer was able to evaluate

over 1,000 compositions per day. In broader studies involving over 43,000 potential compositions, the system successfully reduced the candidate pool to 3,161 for detailed evaluation. This transformed a task that would require approximately two years of manual CALPHAD evaluation (at a rate of 100 compositions per day) into a process completed in under a week. This case study underscores the Simulation Layer's central role in AutoMAT. By integrating rigorous CALPHAD predictions with adaptive AI-guided search, and applying domain-informed constraints to support automation, AutoMAT efficiently explored the high-dimensional compositional space and resolved critical property trade-offs. The final composition, Ti_{81.4}-Al_{16.8}-V_{1.6}-Fe_{0.2}, not only met the performance targets in CALPHAD, but also provided a robust computational foundation for downstream experimental validation. The results demonstrate AutoMAT's capability to accelerate the discovery of high-performance alloys through efficient, autonomous decision-making.

Experimental Validation of Optimized Alloy Composition. Consistent with our focus on as-cast alloys to evaluate intrinsic compositional effects without post-processing, we experimentally validated the optimized composition, Ti_{81.4}-Al_{16.8}-V_{1.6}-Fe_{0.2}, identified by AutoMAT. The ingot morphology is shown in the inset of Fig. 4a. The experimentally measured composition closely matched the predicted values (Supplementary Table 1). Tensile test results shown in Fig. 4a confirmed the success of AutoMAT's prediction and optimization process, with values summarized in Supplementary Table 2. The synthesized alloy exhibited a low density (4.32 g/cm³), satisfying the design requirement of < 4.36 g/cm³, while maintaining a high yield strength of 829 MPa and an impressive high specific strength (202×10^3 Pa m³ per kg) at room temperature. As shown in Fig. 4b and Supplementary Table 3, such yield strength surpasses that of the deformed Al alloys, deformed Mg alloys, and as-cast HEAs, and is comparable to both additive-manufactured titanium alloys and the lightweight Ti_{75.25}Al₂₀Cr_{4.75} shape-memory alloy^{21,23-36}. Notably, this alloy exhibits the highest specific strength among all compared systems, highlighting its strong potential for demanding applications such as the aerospace sector and space applications.

Microstructural characterization revealed promising structural features. In accordance with our calculated solidification path, The XRD result showed that the alloy was composed of α and β phases (Supplementary Fig. 2 and Supplementary Fig. 3). Electron Backscatter Diffraction (EBSD) and Backscattered Electron (BSE) imaging (Fig. 4c) showed an overall lath-like α -grain structure with nano-sized precipitates (Its phase map was shown in Supplementary Fig. 4). High-Angle Annular Dark-Field Scanning Transmission Electron

Microscopy (HADDF-STEM) and the corresponding Energy Dispersive Spectroscopy (EDS) maps (Fig. 4d) indicated these precipitates were Fe- and V-rich (The Compositional profiles recorded across the yellow arrow in Fig. 4d was shown in Supplementary Fig. 5). A dark-field TEM image based on a (010) type superlattice reflection (Fig. 4e) revealed the spatial distribution of the bright β phase. The α phase was observed in the matrix, while the disordered β phase was confined to the nano-sized precipitates (Their chemical compositions were shown in Supplementary Table 4). Moreover, a fully coherent interface between the α matrix and the β precipitates was revealed by the high-resolution TEM (HR-TEM) and the corresponding FFT patterns (Fig. 4f). This microstructure, comprising ultrafine lath-like α -grains and nano-sized β precipitates, is known to be highly beneficial for achieving high strength in titanium alloys³⁷.

As the aerospace and automotive industries pursue greater maneuverability and reduced energy consumption^{38,39}, lightweight structural materials with excellent mechanical properties have attracted increasing attention. Compared to the initial LLM-suggested candidate—Ti-185, a promising low-cost alloy for aviation applications²²—with an experimental density of 4.70 g/cm³ and yield strength of 832 MPa, the final alloy identified by AutoMAT achieved a 8.1% reduction in density while maintaining its yield strength (only a 0.5% decrease). Since their commercial introduction in the 1950s, titanium alloys have maintained relatively stable densities, typically ranging from 4.43 to 4.48 g/cm³⁴⁰, with aerospace-graded alloys falling between 4.37 to 4.56 g/cm³, a range shaped by the persistent trade-off between density and strength⁴¹. AutoMAT's ability to overcome such trade-off highlights its promise for advancing the boundaries of lightweight alloy design. Moreover, lowering alloy density is particularly impactful for commercial aircraft, especially engines weighing 2,000-8,500 kg and composed of 85–95% metallic materials⁴². Given the rising demand for air travel and annual fuel expenditures exceeding US\$180 billion, reducing structural weight translates directly into lower fuel consumption, reduced CO₂ emissions, and enhanced energy efficiency⁴³. Although a decrease in ductility was observed, i.e., 2.3% elongation compared to 6.9% of the reference alloy Ti-185, this trade-off was acceptable given the primary design objectives of high specific strength performance.

Together, these results demonstrate AutoMAT's capability not only to optimize properties within a given alloy system, but also to intelligently select the appropriate system at the ideation stage. The validated outcome underscores the framework's capacity to autonomously deliver materials that satisfy complex, multi-objective criteria, bridging computational design and experimental realization.

Generalizability of AutoMAT. To further demonstrate the generalizability of AutoMAT, particularly its feasibility in high-dimensional design spaces involving more elements, we applied it to a second design task: the discovery of a HEA optimized for higher yield strength. Incorporating the five most commonly investigated elements⁴⁴, the AlCoCrFeNi alloy system was chosen due to its favorable mechanical properties⁴⁵. As the task focused on conventional HEAs, the Ideation Layer was not required to recommend a new alloy family; instead, it proposed Al_{10.5}-Co-Cr-Fe-Ni as the starting point. The Simulation Layer then identified an optimized composition, Al_{14.5}-Co_{27.0}-Cr_{21.5}-Fe_{13.0}-Ni_{24.0} (at%), after five iterations of AI-driven search. This process reduced the candidate pool from over 200,000 possible compositions to fewer than 6,000 candidates for detailed evaluation, compressing simulation time from an estimated ten years of manual effort to under two weeks. Experimental validation confirmed the effectiveness of the recommended composition, achieving an approximate 28.2% improvement in yield strength while maintaining high ductility. Full optimization procedures and characterization results are detailed in Supplementary Notes 3 and 4.

Discussion

A central strength of the AutoMAT framework lies in its generality and transferability, suggesting its potential impact extends far beyond the specific application of alloy discovery demonstrated here. This adaptability is rooted in the modular design of its hierarchical structure and the nature of the tools employed within each layer.

The Ideation Layer offers broad applicability across material domains. It leverages the comprehensive knowledge comprehension and synthesis capabilities of LLMs to extract insights from vast bodies of scientific literature and databases. Its core functionality, identifying promising elemental combinations or material systems based on the keywords of desired property, is not inherently limited to alloys. The scientific foundations of polymers, ceramics, catalysts, biomaterials, and other material classes are similarly well-documented in textual formats accessible to LLMs. With tailored prompt engineering, the Ideation Layer could rapidly generate candidate hypotheses for virtually any materials discovery challenge underpinned by a substantial literature base. Its ability to efficiently convert unstructured domain knowledge into structured machine-readable suggestions makes it a powerful and domain-agnostic front-end for diverse materials discovery pipelines. In this sense, the Ideation Layer functions as a general-purpose scientific reasoning engine, capable of catalyzing hypothesis generation across the entire landscape of materials science.

The Simulation Layer further enhances platform flexibility through its simulation-engine-agnostic structure. In this study, we employed CALPHAD, which is well-suited for efficiently predicting phase stability and thermodynamic properties in metallic systems. However, the Simulation Layer's functional role, as a physics-based evaluator and optimizer of candidate materials, remain constant regardless of the simulation engine used. For different material classes or design targets, CALPHAD could be replaced with first-principles methods such as Density Functional Theory (DFT), typically implemented using software packages like VASP (Vienna Ab initio Simulation Package). This would enable evaluations of properties where quantum-level accuracy is essential, such as electronic band structure, surface energetics, and defect formation energies, which are critical for the design of functional materials like semiconductors and catalysts. Beyond DFT, other simulation techniques could be integrated as needed: Molecular Dynamics (MD) for modeling time-evolving phenomena such as transport property and diffusion, or Finite Element Analysis (FEA) for macro-scale mechanical behavior. This "plug-and-play" flexibility allows AutoMAT to be easily reconfigured to incorporate the most appropriate simulation methods for the task at hand. The Simulation Layer thus serves as a robust middle tier in the architecture, one that is both methodologically rigorous and structurally adaptable.

Together, the transferable Ideation Layer and the adaptable Simulation Layer form the computational backbone of AutoMAT. Although the Validation Layer necessarily requires domain-specific experimental techniques, the modularity of the upstream layers allows broad reusability across materials domains. This architecture transforms AutoMAT from a purpose-built alloy pipeline into a general-purpose framework for autonomous materials discovery. By integrating knowledge extraction, physics-informed simulation, and automated optimization within a hierarchical, modular structure, AutoMAT presents a scalable and forward-compatible solution. It is not only capable of accelerating existing design tasks but also of evolving with emerging advances in LLMs, surrogate modeling, or simulation tools. Looking ahead, the architecture lays the groundwork for an even more transformative capability: closing the loop between validation and ideation. Although the current workflow is unidirectional, future iterations could leverage experimental outcomes to automatically refine initial hypotheses and simulation parameters, creating a truly autonomous, self-correcting system for materials discovery. In doing so, AutoMAT positions itself as a blueprint for next-generation, AI-driven materials innovation—paving the way for autonomous design across the diverse and expanding frontier of materials science.

Methods

Ideation Layer

OpenAI's GPT-4o model (accessed via API) was utilized for all natural language processing and knowledge extraction tasks within the Ideation Layer. GPT-4o was selected for its advanced capabilities in natural language understanding, complex reasoning, and information extraction from extensive textual corpora at the time of the study, which were deemed critical for effectively navigating and interpreting materials science literature and specialized handbooks.

User-defined property targets, such as desired yield strength (e.g., approaching 850 MPa), maximum density (e.g., $< 4.36 \text{ g/cm}^3$), and elemental cost or exclusion constraints, were formulated into structured prompts to guide GPT-4o. All prompt templates were set up in advance with blanks in them. When the user inputs the requirements, their requirements will be filled into the blanks to complete the prompt. All prompt templates can be found in Supplementary Note 2.

Simulation Layer

All thermodynamic calculations and properties predictions were conducted using Thermo-Calc software (version 2024b). Automation of these computations was achieved through the TCPython package interfacing with the server. The TCHEA7 thermodynamic database underpinned all calculations, supplying the Gibbs energy descriptions for constituent phases essential for determining equilibrium states.

The initial step in all calculations involved computing phase volume fractions. For this, the Scheil module was utilized to generate Scheil solidification curves. These curves represent the phase formation during solidification by sampling numerous points between a fraction solid of 0 and 1, thereby identifying the corresponding phases at each interval. The system incorporates a process to identify new phases as the temperature drops and filter noise from the Scheil curve, yielding accurate final phase volumes. Apart from the composition itself, temperature is the only critical parameter, which was set to 3000 °C to ensure complete melting of the alloys under investigation.

The specific property calculations were performed with established phase volumes. Densities, for both individual phases and the overall alloy, were derived from the molar volumes and compositions of the equilibrium phases. The yield strength of candidate alloys

was predicted via the property model calculation module. For these yield strength calculations, intrinsic strength for the pure elements, solid solution strengthening, and grain boundary strengthening were enabled, while precipitation strengthening was disabled. A grain size of 100 μm was specified for the grain boundary strengthening contribution.

Validation Layer (Experimental)

Ingots were prepared by arc-melting the high-purity elements of Ti, Al, V and Fe (larger than 99.99 wt.%). The ingots were re-melted seven times to promote homogeneity under high-purity argon atmosphere. To determine their mechanical properties, flat, dog-bone-shaped tensile samples with a gauge length of 8 mm, a width of 2 mm and a thickness of 1 mm were extracted from the alloys by using electrical discharge machining. Uniaxial tensile tests were conducted using a ETM503C universal testing machine at a strain rate of $1 \times 10^{-3} \text{ s}^{-1}$ at room temperature, and each condition was repeated at least three times. The density of the alloys at each condition was measured 5 times via SD-200L densimeter. The chemical composition of each ingot was measured via ICP method. Crystal orientation and microstructure observation were performed by Gemini 300 equipped with Symmetry S3 electron backscattered diffraction detector. TEM analysis was conducted using a ThermoFisher Talos F200X fitted with a STEM-EDS detector to investigate their crystal structure, elemental compositions, and interfacial features between different phases at 200 kV.

Data availability

The authors declare that all relevant data are included in the paper and its Supplementary Information.

Declaration of competing interest

The authors declare that they have no known competing financial interests or personal relationships that could have appeared to influence the work reported in this paper.

Acknowledgements

This work was supported by the National Research Foundation Singapore and DSO National Laboratories under the AI Singapore Programme (AISG Award No: AISG2-GC-2023-009). We acknowledge Thermo-Calc for providing the shrinkage calculations.

Author contributions

P.Y. and C.Z. contributed equally to this work. B.A., Z.L., and B.T. conceived and supervised the project. P.Y. designed the AutoMAT framework and developed the algorithms. C.Z. synthesized the samples and performed mechanical and structural characterizations. Z.Z. contributed to the CALPHAD calculations. X.W. and Y.D. supported the development of the AI search algorithm. Y.L. assisted with data analysis. P.Y., C.Z., and B.T. co-wrote the manuscript. All authors discussed the results and contributed to the final manuscript.

References

1. Pollock, T. M. Alloy design for aircraft engines. *Nat. Mater.* **15**, 809–815 (2016).
2. Froes, F. H., Friedrich, H., Kiese, J. & Bergoint, D. Titanium in the family automobile: The cost challenge. *JOM* **56**, 40–44 (2004).
3. Jiang, S. *et al.* Ultrastrong steel via minimal lattice misfit and high-density nanoprecipitation. *Nature* **544**, 460–464 (2017).
4. Yan, Y.-Q. *et al.* Ductilization of 2.6-GPa alloys via short-range ordered interfaces and supranano precipitates. *Science* **387**, 401–406 (2025).
5. Rao, Z., Springer, H., Ponge, D. & Li, Z. Combinatorial development of multicomponent Invar alloys via rapid alloy prototyping. *Materialia* **21**, 101326 (2022).
6. Pei, Z., Yin, J., Liaw, P. K. & Raabe, D. Toward the design of ultrahigh-entropy alloys via mining six million texts. *Nat. Commun.* **14**, 54 (2023).
7. George, E. P., Raabe, D. & Ritchie, R. O. High-entropy alloys. *Nat. Rev. Mater.* **4**, 515–534 (2019).
8. Rao, Z. *et al.* Machine learning-enabled high-entropy alloy discovery. *Science* **378**, 78–85 (2022).
9. Merchant, A. *et al.* Scaling deep learning for materials discovery. *Nature* **624**, 80–85 (2023).
10. Li, K. *et al.* Probing out-of-distribution generalization in machine learning for materials. *Commun. Mater.* **6**, 1–10 (2025).
11. Batra, R., Song, L. & Ramprasad, R. Emerging materials intelligence ecosystems propelled by machine learning. *Nat. Rev. Mater.* **6**, 655–678 (2021).
12. Pei, Z., Yin, J., Neugebauer, J. & Jain, A. Towards the holistic design of alloys with large language models. *Nat. Rev. Mater.* **9**, 840–841 (2024).
13. Yin, L. *et al.* CALPHAD accelerated design of advanced full-Zintl thermoelectric device. *Nat. Commun.* **15**, 1468 (2024).
14. Mao, H., Chen, H.-L. & Chen, Q. TCHEA1: A thermodynamic database not limited for “high entropy” alloys. *J. Phase Equilibria Diffus.* **38**, 353–368 (2017).
15. Feng, R. *et al.* High-throughput design of high-performance lightweight high-entropy alloys. *Nat. Commun.* **12**, 4329 (2021).
16. Wei, S., Ma, Y. & Raabe, D. One step from oxides to sustainable bulk alloys. *Nature* **633**, 816–822 (2024).

17. Raabe, D. The materials science behind sustainable metals and alloys. *Chem. Rev.* **123**, 2436–2608 (2023).
18. Scheil, E. Bemerkungen zur Schichtkristallbildung. *Int. J. Mater. Res.* **34**, 70–72 (1942).
19. Andersson, J.-O., Helander, T., Höglund, L., Shi, P. & Sundman, B. Thermo-Calc & DICTRA, computational tools for materials science. *Calphad* **26**, 273–312 (2002).
20. Hu, Q.-M. & Yang, R. The endless search for better alloys. *Science* **378**, 26–27 (2022).
21. Song, Y. *et al.* A lightweight shape-memory alloy with superior temperature-fluctuation resistance. *Nature* **638**, 965–971 (2025).
22. Boyer, R., Welsch, G. & Collings, E. Materials Properties Handbook: Titanium Alloys. in (1994).
23. Gludovatz, B. *et al.* A fracture-resistant high-entropy alloy for cryogenic applications. *Science* **345**, 1153–1158 (2014).
24. Achieving ultrahigh fatigue resistance in AlSi10Mg alloy by additive manufacturing | Nature Materials. <https://www.nature.com/articles/s41563-023-01651-9>.
25. Lei, Z. *et al.* Enhanced strength and ductility in a high-entropy alloy via ordered oxygen complexes. *Nature* **563**, 546–550 (2018).
26. Yan, C. *et al.* Evading strength-corrosion trade off in Mg alloys via dense ultrafine twins. *Nat. Commun.* **12**, 4616 (2021).
27. Liu, D. *et al.* Exceptional fracture toughness of CrCoNi-based medium- and high-entropy alloys at 20 kelvin. *Science* **378**, 978–983 (2022).
28. Pan, Q. *et al.* Gradient cell-structured high-entropy alloy with exceptional strength and ductility. *Science* **374**, 984–989 (2021).
29. Shi, P. *et al.* Hierarchical crack buffering triples ductility in eutectic herringbone high-entropy alloys. *Science* **373**, 912–918 (2021).
30. Xue, H. *et al.* Highly stable coherent nanoprecipitates via diffusion-dominated solute uptake and interstitial ordering. *Nat. Mater.* **22**, 434–441 (2023).
31. Cook, D. H. *et al.* Kink bands promote exceptional fracture resistance in a NbTaTiHf refractory medium-entropy alloy. *Science* **384**, 178–184 (2024).
32. Song, T. *et al.* Strong and ductile titanium–oxygen–iron alloys by additive manufacturing. *Nature* **618**, 63–68 (2023).

33. Jiang, S. *et al.* Structurally complex phase engineering enables hydrogen-tolerant Al alloys. *Nature* **641**, 358–364 (2025).
34. Zhu, Q. *et al.* Towards development of a high-strength stainless Mg alloy with Al-assisted growth of passive film. *Nat. Commun.* **13**, 5838 (2022).
35. Zhang, J. *et al.* Ultrauniform, strong, and ductile 3D-printed titanium alloy through bifunctional alloy design. *Science* **383**, 639–645 (2024).
36. Yang, H. *et al.* Alloying design of biodegradable zinc as promising bone implants for load-bearing applications. *Nat. Commun.* **11**, 401 (2020).
37. Qu, Z. *et al.* High fatigue resistance in a titanium alloy via near-void-free 3D printing. *Nature* **626**, 999–1004 (2024).
38. Zhang, X., Chen, Y. & Hu, J. Recent advances in the development of aerospace materials. *Prog. Aerosp. Sci.* **97**, 22–34 (2018).
39. Williams, J. C. & Starke, E. A. Progress in structural materials for aerospace systems. *Acta Mater.* **51**, 5775–5799 (2003).
40. Singh, P., Pungotra, H. & Kalsi, N. S. On the characteristics of titanium alloys for the aircraft applications. *Mater. Today Proc.* **4**, 8971–8982 (2017).
41. Polmear, I., StJohn, D., Nie, J.-F. & Qian, M. *Light Alloys: Metallurgy of the Light Metals*. (Butterworth-Heinemann, 2017).
42. Schafrik, R. & Sprague, R. Siga of gas turbine materials: Part I. *Adv. Mater. Amp Process.* **162**, 33–37 (2004).
43. Boyer, R. R. Aerospace applications of beta titanium alloys. *JOM* **46**, 20–23 (1994).
44. Miracle, D. B. & Senkov, O. N. A critical review of high entropy alloys and related concepts. *Acta Mater.* **122**, 448–511 (2017).
45. Chandra, S., Wang, C., Tor, S. B., Ramamurty, U. & Tan, X. Powder-size driven facile microstructure control in powder-fusion metal additive manufacturing processes. *Nat. Commun.* **15**, 3094 (2024).

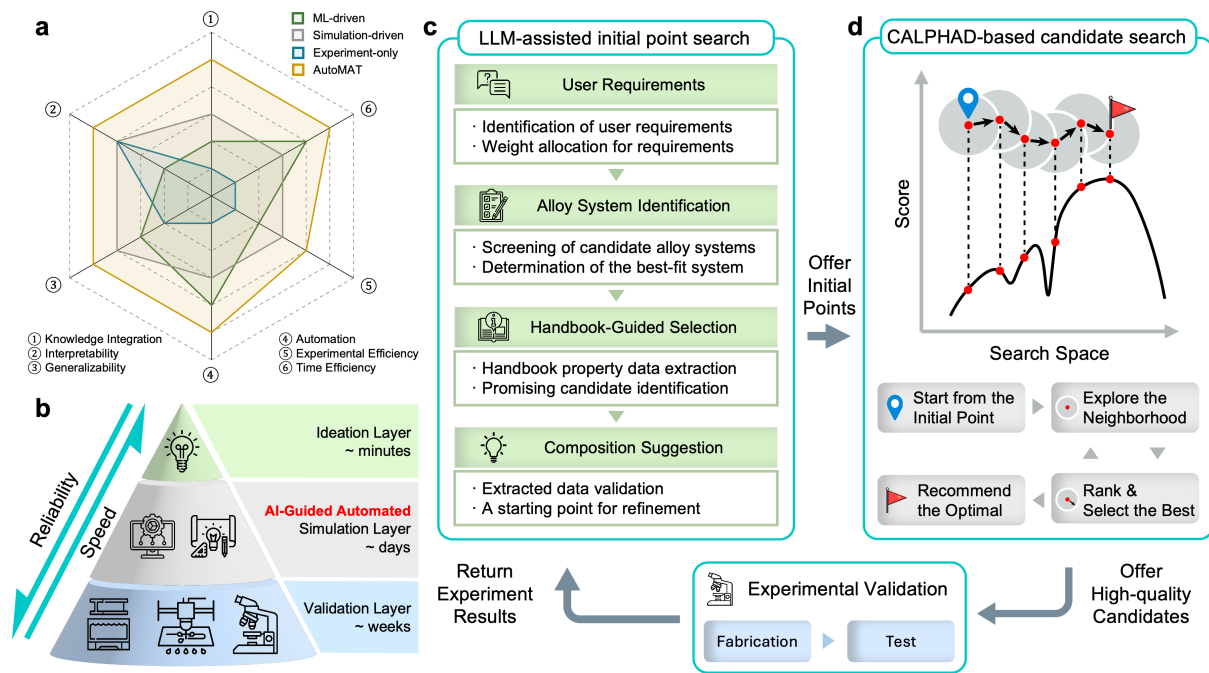


Fig. 1 | AutoMAT framework: architecture and performance comparison. **a**, Radar chart comparing the performance of AutoMAT with existing methods across six key dimensions: knowledge integration, interpretability, generalizability, automation, experimental efficiency, and time efficiency. Scoring criteria are detailed in Supplementary Note 1. **b**, Overview of AutoMAT’s three-tier structure: the Ideation Layer, the Simulation Layer, and the Validation Layer. **c**, In the Ideation Layer, LLMs assist in alloy system selection and initial composition identification based on user-defined property targets, handbook data, and known alloy systems. **d**, The Simulation Layer applies CALPHAD-based modeling to explore compositional neighborhoods, rank candidates, and recommend optimal compositions for experimental validation.

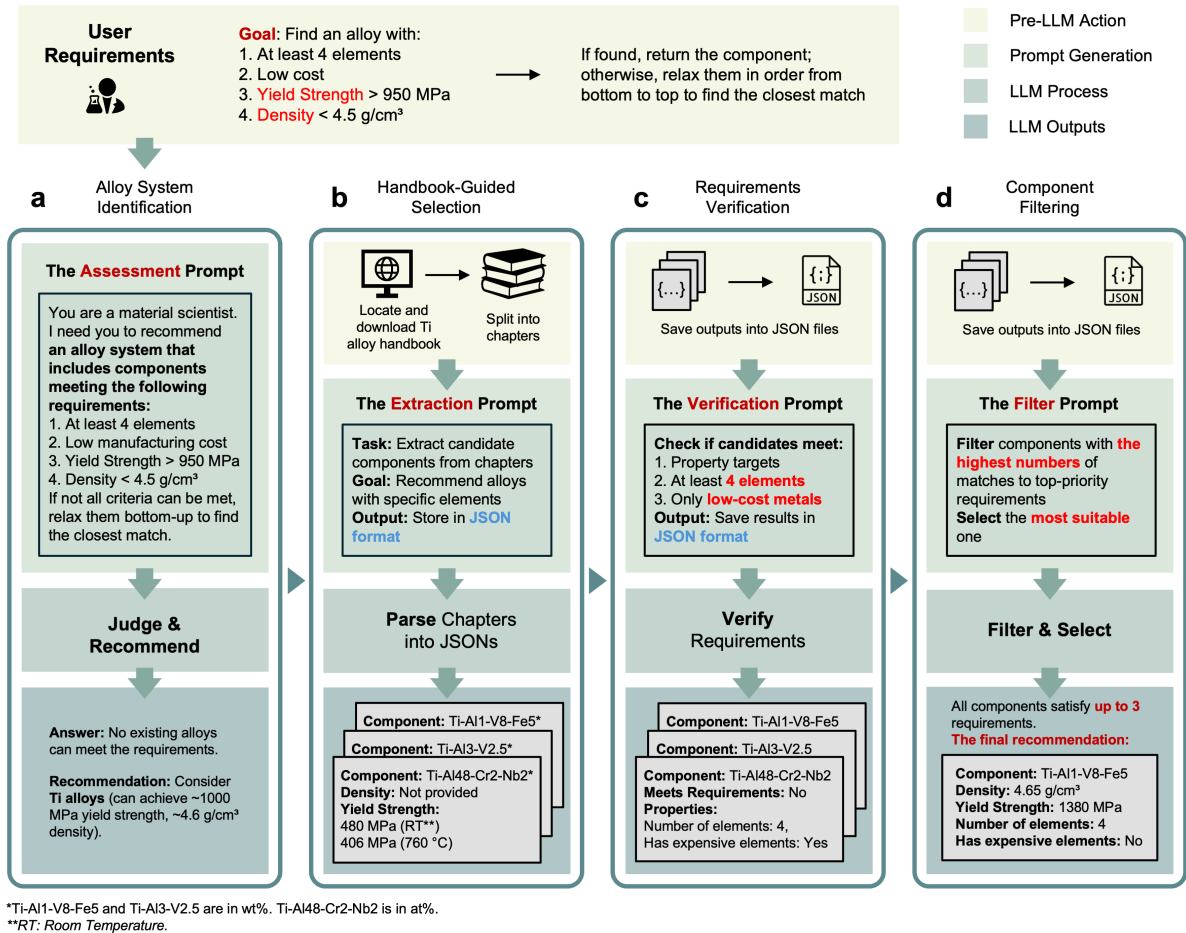


Fig. 2 | Stepwise process of the Ideation Layer in AutoMAT. **a**, Alloy system identification proposes an alloy system that best matches the user-defined requirements. **b**, Handbook-guided selection retrieves the alloy handbook for the chosen system and extracts all possible alloy components. **c**, Requirements verification evaluates whether each candidate meets the specified property constraints. **d**, Component filtering ranks candidates based on the degree of requirements satisfaction and selects the most promising composition.

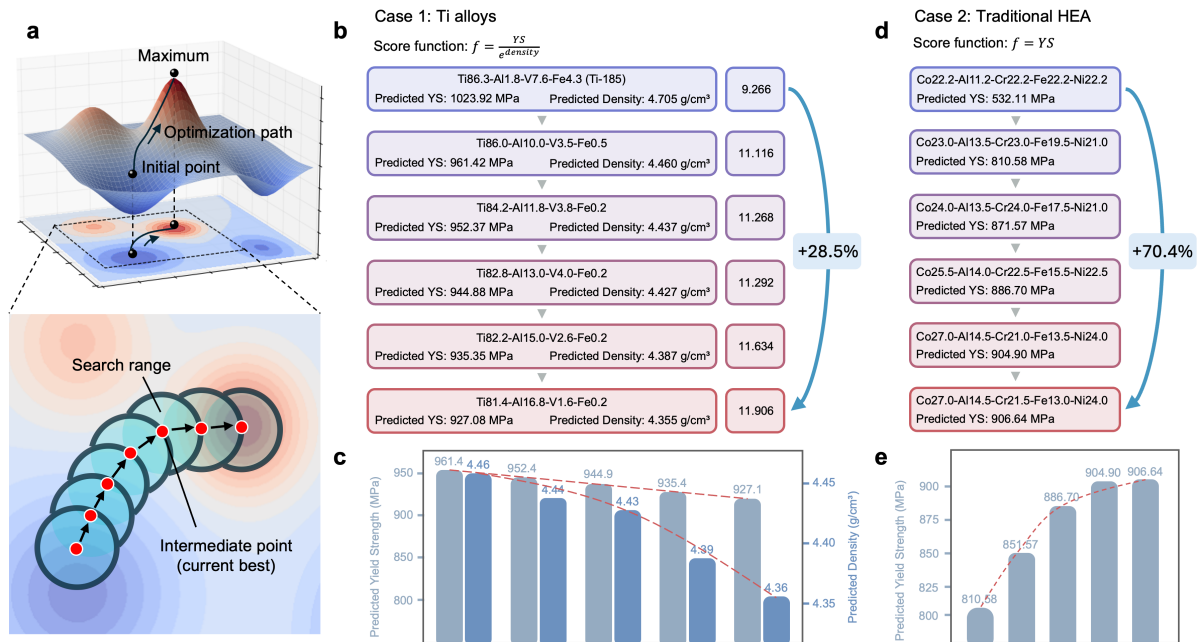


Fig. 3 | AI-guided CALPHAD optimization and search trajectories in AutoMAT. a, AI-driven search explores the compositional design space by iteratively sampling within a fixed search range around the current candidate. **b**, Search trajectory for Case 1, showing a 28.5% score improvement as the model iteratively proposes alloys with enhanced yield strength and reduced density. **c**, Predicted yield strength and density across candidate alloys in Case 1, demonstrating a moderate reduction in yield strength alongside a significant reduction in density. **d**, Search trajectory for Case 2, achieving a 70.4% improvement through identification of compositions with markedly higher mechanical performance. **e**, Predicted yield strength for Case 2, highlighting substantial improvement relative to the initial point.

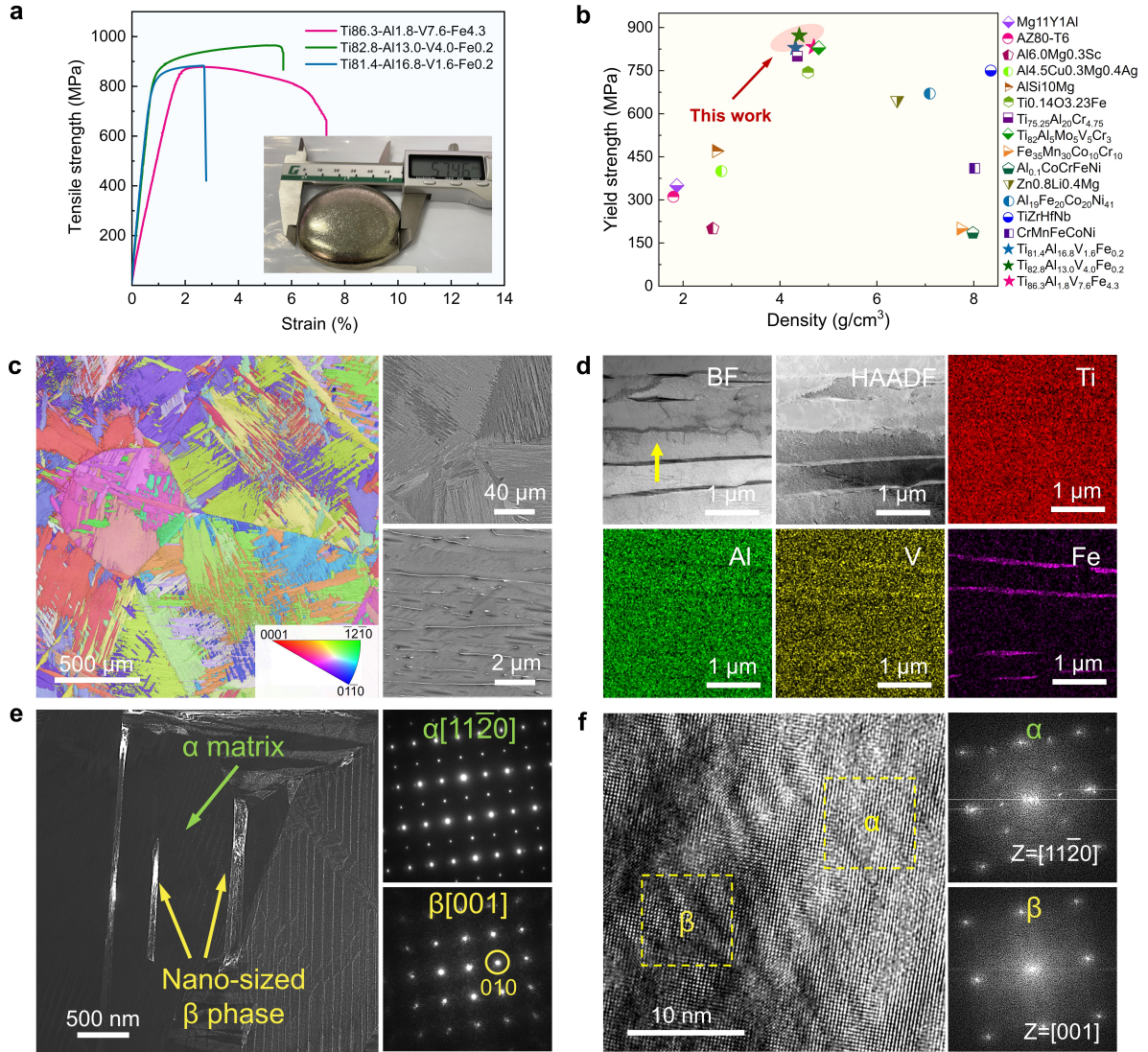


Fig. 4 | Mechanical performance and microstructural characterization of the as-cast titanium alloys. **a**, Representative engineering stress-strain curves from tensile testing; the inset shows the ingot morphology. **b**, Comparison of yield strength and density between the current study and previously reported alloys^{21,23–36}. **c**, The EBSD inverse pole figure (IPF) color map; right panels display BSE images at different magnifications. **d**, Bright-field TEM image, HAADF-STEM image, and EDS mappings of the α - β region. **e**, Dark-field TEM image made from the (010) superlattice spot marked by the yellow circle showing the α matrix and lighted-up β phases. Right panels show selected area diffraction (SAD) patterns from $[001]_{\beta}$ ZA and $[1120]_{\alpha}$ zone axes. **f**, High-resolution TEM image of the α - β region, with their corresponding FFT images displayed on the right.

Supplementary Information for

AutoMAT: A Hierarchical Framework for Autonomous High-Entropy

Alloy Discovery

Penghui Yang^{1,6}, Chendong Zhao^{2,6}, Bijun Tang^{2✉}, Zhonghan Zhang¹, Xinrun Wang^{3✉},
Yanchen Deng¹, Yuhao Lu¹, Cuntai Guan¹, Zheng Liu^{2,4,5✉}, Bo An^{1✉}

¹College of Computing and Data Science, Nanyang Technological University, Singapore 639798, Singapore

²School of Materials Science and Engineering, Nanyang Technological University, Singapore 639798, Singapore

³School of Computing and Information Systems, Singapore Management University, Singapore 188065

⁴CINTRA CNRS/NTU/THALES, UMI 3288, Research Techno Plaza, 50 Nanyang Drive, Border X Block, Level 6, Singapore 637553, Singapore

⁵Institute for Functional Intelligent Materials, National University of Singapore, Singapore, Singapore

⁶These authors contributed equally: Penghui Yang, Chendong Zhao

✉E-mail: bjtang@ntu.edu.sg; xrwang@smu.edu.sg; z.liu@ntu.edu.sg; boan@ntu.edu.sg

Table of Contents

Supplementary Notes

Supplementary Note 1: Scoring rules of the radar chart

Supplementary Note 2: Prompt and examples of LLM responses in the Ideation Layer

Supplementary Note 3: Details of the case study on conventional HEAs in the Simulation Layer

Supplementary Note 4: Experimental validation of the Simulation Layer based on AlCoCrFeNi alloy system

Supplementary Figures

Supplementary Fig. 1 | Process of using Scheil solidification to improve the reliability of the prediction in the yield strength

Supplementary Fig. 2 | Calculated solidification path of the $\text{Ti}_{81.4}\text{Al}_{16.8}\text{V}_{1.6}\text{Fe}_{0.2}$ alloy by the Scheil model

Supplementary Fig. 3 | XRD pattern of the as-cast $\text{Ti}_{81.4}\text{Al}_{16.8}\text{V}_{1.6}\text{Fe}_{0.2}$ alloy

Supplementary Fig. 4 | The corresponding EBSD phase map of Fig. 4c

Supplementary Fig. 5 | Compositional profiles recorded across the yellow arrow in Fig. 4d, the purple region indicate the Fe- and V-rich precipitate

Supplementary Fig. 6 | Typical engineering tensile stress-strain curves of the as-cast HEAs

Supplementary Tables

Supplementary Table 1 | Chemical compositions of the as-cast titanium alloys

Supplementary Table 2 | Tensile properties of the as-cast titanium alloys

Supplementary Table 3 | Theoretical and experimental yield strength of the alloys in Fig. 4b

Supplementary Table 4 | The EDS chemical compositions of the α phase and β phase

Supplementary Table 5 | Chemical compositions of the as-cast HEAs

Supplementary Table 6 | Tensile properties of the as-cast HEAs

Supplementary References

Supplementary Notes

Supplementary Note 1: Scoring rules of the radar chart

- Knowledge Integration
 - Definition: Refers to the method's ability to systematically utilize and integrate existing human knowledge, such as scientific literature, manuals, and databases.
 - Scoring Criteria:
 - 1 point: Hardly uses existing knowledge bases; mainly relies on intuition or raw data.
 - 2 points: Indirectly utilizes knowledge through training data; unable to actively query.
 - 3 points: Depends on formalized knowledge bases (e.g., thermodynamic databases).
 - 4 points: Can combine multiple formalized knowledge bases for decision-making.
 - 5 points: Actively and systematically integrates unstructured textual knowledge (literature) and structured data (manuals, databases).
- Interpretability
 - Definition: Each decision step and the final outcome provided by the method are clearly traceable and supported by explicit physical or chemical principles.
 - Scoring Criteria:
 - 1 point: Completely "black-box"; decision processes cannot be explained.
 - 2 points: Partially interpretable; critical steps depend on hard-to-understand correlations.
 - 3 points: Results interpretable, but the deduction process is indirect and convoluted.
 - 4 points: Most decisions based on explicit physical models (e.g., thermodynamics).
 - 5 points: Every step, from initial selection to final optimization, is supported by a clear, intuitive physical/chemical logical chain.

- Generalizability
 - Definition: The framework's ability and associated cost to transition from one materials discovery problem (e.g., specific alloy systems or properties) to a completely different materials discovery problem. High generalizability indicates universal core logic and low transition cost.
 - Scoring Criteria:
 - 1 point: Highly problem-specific, almost impossible to transfer; relies on implicit, non-transferable expert knowledge.
 - 2 points: Requires substantial time investment to learn; explicit but non-transferable expert knowledge.
 - 3 points: Transferable but heavily dependent on extensive data from the specific domain. Transferring requires expensive new data collection and model training.
 - 4 points: Framework depends on a single type of physical model/database within a specific domain. Transfer depends on the existence or development of similar dedicated computational tools/databases in the new domain.
 - 5 points: Framework is modular; the transfer process is clear, involving only replacement of core computational modules (e.g., replacing CALPHAD with DFT) while maintaining the overall logic.

- Automation
 - Definition: The degree to which tasks in the discovery process can be automatically executed by machines or software, reducing human intervention.
 - Scoring Criteria:
 - 1 point: Completely manual; every step requires human operation and decision-making.
 - 2 points: Partial computational automation; most tasks still require human intervention.
 - 3 points: Partial computational automation; human intervention required to connect workflow steps.

- 4 points: Most computational workflows automated; initial parameters and interpretation of results require human input.
- 5 points: Most steps in the closed loop are automated, with human involvement primarily for supervision.
- Experimental Efficiency
 - Definition: The number and complexity of experiments required throughout the discovery process to identify the final candidate alloy.
 - Scoring Criteria:
 - 1 point: Extremely high; requires numerous and complex experimental series.
 - 2 points: Relatively high; requires multiple iterative experiments for training or validation.
 - 3 points: Moderate; validation experiments needed for a set of candidate materials.
 - 4 points: Relatively low; validation needed only for a few (<5) final candidate materials.
 - 5 points: Extremely low; ideally only the final 1-2 optimal candidates require validation.
- Time Efficiency
 - Definition: The time required from project initiation to obtaining validated candidate alloys that meet the specified requirements.
 - Scoring Criteria:
 - 1 point: Extremely slow, typically taking several years.
 - 2 points: Slow, taking more than one year.
 - 3 points: Moderate, ranging from several months to one year.
 - 4 points: Relatively fast, usually completed within three months.
 - 5 points: Extremely fast, theoretically able to complete a discovery cycle within weeks.

Supplementary Note 2: Prompt and examples of LLM responses in the Ideation Layer

Step 1 Alloy System Identification

User:

You are a material scientist. I need you to recommend an alloy system that includes components meeting the following requirements:

1. At least 4 elements
2. Low manufacturing cost
3. Yield Strength > 950 MPa
4. Density < 4.5 g/cm³

If not all criteria can be met, relax them bottom-up to find the closest match.

Assistant (LLM): To meet your tough targets, you need lightweight and high-strength systems. Here are some promising directions:

1. Titanium Alloys

Density: ~4.43 g/cm³

Yield Strength: Often exceeds 800 MPa, with certain grades like Ti-6Al-4V reaching yield strengths of 900–1000 MPa.

Composition: Primarily titanium, aluminum (6%), and vanadium (4%) in wt%.

Performance: Commonly used in aerospace and biomedical applications due to their excellent strength-to-weight ratio and corrosion resistance.

2. Aluminum-Lithium Alloys

Density: Typically around 2.6–2.8 g/cm³

Yield Strength: Exceeds 800 MPa in some grades, especially when heat-treated.

Composition: Aluminum, lithium (1–3%), with trace amounts of other elements like copper or magnesium.

Performance: Used in aerospace to reduce weight while maintaining strength, particularly in aircraft fuselage and wings.

3. Magnesium Alloys

Density: Around 1.74–2 g/cm³

Yield Strength: Newer magnesium alloys have been developed with yield strengths exceeding 300 MPa and can reach up to 800 MPa under the right conditions.

Composition: Magnesium combined with elements like aluminum, zinc, and rare earth elements.

Performance: Magnesium alloys are of particular interest for automotive and electronics industries where weight savings are critical.

Step 2 Handbook-Guided Selection

User: I have provided a chapter in a material handbook in PDF format. The chapter contains information about the properties and components of various alloys. I would like you to act as a material scientist and help me analyze the chapters.

1. Your Task:

Retrieve all the components that have the exact information of Yield Strength and Density in the book.

2. Expected Output:

List the recommended alloy components along with their corresponding properties (density, yield strength, etc.). Please retrieve all the results with information of Alloy Component, Density (g/cm^3) and Yield Strength (MPa) in a json format.

Assistant (just one example is shown here): Sure! Based on the provided content from the PDF, here is the information in JSON format regarding the alloys with their corresponding Density and Yield Strength:

```
```json
[
 {
 "Alloy Component": "Corona 5",
 "Density (g/cm^3)": 4.54,
 "Yield Strength (MPa)": 825
 },
 {
```

```
"Alloy Component": "Ti-6Al-4V",
"Density (g/cm^3)": 4.43,
"Yield Strength (MPa)": 795
}
]
``
```

This JSON format lists the relevant alloy components and their properties as you requested.

### Step 3 Requirements Verification

**User:** I have provided a component extracted from a material handbook. The contents contain information about the properties and components of various alloys. I would like you to act as a material scientist and help me analyze the contents.

Your Task:

Evaluate the alloy component based on the primary requirements provided. Your task is to determine if it meets the primary requirements.

Primary Requirements (Must-Have):

- The component should contain four elements or more.
- The component should include low-cost metals such as Al, Fe and exclude any expensive metals such as Zr, Mo.

Expected Output: Output whether it meets the primary requirements. If it does, specify the properties (number of elements and cost-related details). If not, state which requirement(s) it fails to meet.

Format: Please present the result in a clear json format as follows:

```
``json
{
 "Alloy Component": [Name of Component]
 "Meets Requirements": [Yes/No]
 "Properties": {
```

```
"Number of elements": [Number]
"Has expensive elements or not": [Yes/No]
}
}
...
```

**Assistant (just one example is shown here):**

```
```json
{
  "Alloy Component": "Ti-6Al-4V",
  "Meets Requirements": "No",
  "Properties": {
    "Number of elements": 3,
    "Has expensive elements or not": "No"
  }
}
...
```
```

**Explanation:**

- Ti-6Al-4V is a titanium alloy that primarily consists of titanium (Ti), aluminum (Al), and vanadium (V), making it a three-element alloy.
- It does not meet the requirement of containing four or more elements.
- While it includes aluminum, a low-cost metal, it does not contain any explicitly listed expensive metals like zirconium (Zr) or molybdenum (Mo). Therefore, it does not have expensive elements. However, titanium itself is generally considered a relatively expensive material.

**Step 4 Component Filtering**

**User:** I have provided some filtered contents from a material handbook. The contents contain information about the properties and components of various alloys. I would like you to act as a material scientist and help me analyze the contents.

1. Your Task:

Recommend the relevant alloy components and their properties that meet my requirements.

2. Property Requirements:

Based on the filtered data, recommend alloy components that meet the following property requirements:

Requirements (Nice-to-Have):

- Have clear and unambiguous components.
- Density smaller than 3.8 (g/cm<sup>3</sup>).
- Yield Strength larger than 1000 (MPa).

You need to first list all the components that satisfy the primary requirements, and then choose those that meet the requirements.

If no information in the document(s) fully satisfies all the requirements, try to recommend components that satisfies as much requirements as possible.

For requirements that are satisfied by the components, it is encouraged to exceed the requirements so that we can have more space for further modification.

For components that have the same performance on one requirement, prefer those perform better on other requirements.

3. Expected Output:

List the recommended alloy components along with their corresponding properties (density, yield strength, etc.).

Then point out the most recommended one.

4. Format:

Please present the results in a clear table format, with columns for:

- Alloy Component
- Density (g/cm<sup>3</sup>)

- Yield Strength (MPa)
- Number of elements
- Has expensive elements or not

**Assistant:** To address the property requirements specified, I will begin by analyzing the components within the list provided and check how they align with your stated conditions:

Requirements:

- Density smaller than 3.8 g/cm<sup>3</sup>
- Yield Strength larger than 1000 MPa
- Clear and unambiguous component

Upon reviewing the retrieved contents, none of the alloy components meets the exact requirement of having a density smaller than 3.8 g/cm<sup>3</sup>. However, I can identify those components which have the highest potential, exceeding in yield strength and performing best based on the available properties.

Here is the list of alloy components meeting or exceeding the highest possible criteria of yield strength:

| Alloy              | Density (g/cm <sup>3</sup> ) | Yield strength (MPa) | Number of elements | Has expensive elements or not |
|--------------------|------------------------------|----------------------|--------------------|-------------------------------|
| Ti-8V-5Fe-1Al      | 4.65                         | 1380                 | 4                  | No                            |
| Ti-10V-2Fe-3Al     | 4.65                         | 1240                 | 4                  | No                            |
| Ti-15V-3Cr-3Al-3Sn | 4.76                         | 1165                 | 5                  | No                            |
| Ti-6-22-22S Billet | 4.65                         | 1089                 | 4                  | No                            |
| Ti-15-3 (Aged)     | 4.76                         | 1025                 | 4                  | No                            |

Recommendation:



Since none of the alloys meets the density requirement, we focus instead on yield strength performance. Here are the top performers based on yield strength:

- **Ti-1Al-8V-5Fe** (wt.%): This component provides the highest yield strength of 1380 MPa among the listed alloys, with moderate density and four elements, making it versatile given its absence of expensive elements.

- **Ti-3Al-10V-2Fe** (in wt.%, Yield strength: 1240 MPa): If prioritized by yield strength while maintaining clarity in the component composition, this is a strong candidate.

Based on the yield strength performance, the **most recommended alloy** is **Ti-1Al-8V-5Fe**, due to its highest yield strength and moderately favorable density, aligning with your emphasis on exceeding requirements.

While all these recommendations don't fully meet your original request for density, the listed alloys potentially provide excellent yield strength characteristics.

### **Supplementary Note 3: Details of the case study on conventional HEAs in the Simulation Layer**

In the case of conventional HEAs, the initial candidate Al<sub>0.5</sub>-Co-Cr-Fe-Ni was passed to the Simulation Layer for optimization. Given the candidate's relatively low initial predicted yield strength of 532.11 MPa, the primary objective was to maximize this property. The Simulation Layer initiated its autonomous pipeline by leveraging CALPHAD-based methodologies for precise thermodynamic and physical property predictions. Its core strategy was an AI-driven iterative neighborhood search, which efficiently explored the compositional space, initially around the starting HEA and subsequently around the best compositions identified in each iteration.

At each iteration, CALPHAD simulations were performed to predict key properties, with a focus on yield strength, which was calculated based on the volume fractions of individual phases predicted by CALPHAD. Since the system needed to optimize a single objective yield strength, the comparison between candidate compositions was straightforward. Specifically, we defined the score function as  $f = \text{Yield Strength (MPa)}$ , as shown in Fig. 3d. This score function directly guided the search toward alloys with the highest possible mechanical strength.

The algorithm deployed a stable step size of 0.5 for local optimization around the best-performing compositions. All the search steps are shown below:

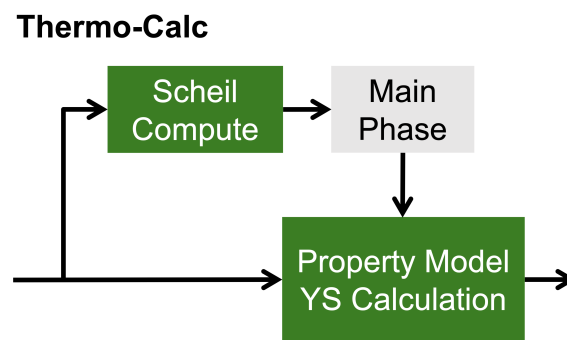
- Step 1: Co23.0-Al13.5-Cr23.0-Fe19.5-Ni21.0 → YS = 810.58 MPa.
- Step 2: Co24.0-Al13.5-Cr24.0-Fe17.5-Ni21.0 → YS = 871.57 MPa.
- Step 3: Co25.5-Al14.0-Cr22.5-Fe15.5-Ni22.5 → YS = 886.70 MPa.
- Step 4: Co27.0-Al14.5-Cr21.0-Fe13.5-Ni24.0 → YS = 904.90 MPa.
- Final step: Co27.0-Al14.5-Cr21.5-Fe13.0-Ni24.0 → YS = 906.64 MPa.

Over the course of five refinement iterations, the simulation converged on a composition that significantly enhanced the target property. The final composition, Co27.0-Al14.5-Cr21.5-Fe13.0-Ni24.0, achieved a predicted yield strength of 906.64 MPa, representing a 70.4% improvement over the initial candidate. This case study underscores the Simulation Layer's central role in AutoMAT. By integrating rigorous CALPHAD predictions with adaptive AI-guided search, and applying domain-informed constraints to support automation, AutoMAT efficiently explored the high-dimensional compositional space to achieve a targeted design objective. The results demonstrate AutoMAT's capability to accelerate the discovery of high-performance alloys through efficient, autonomous decision-making.

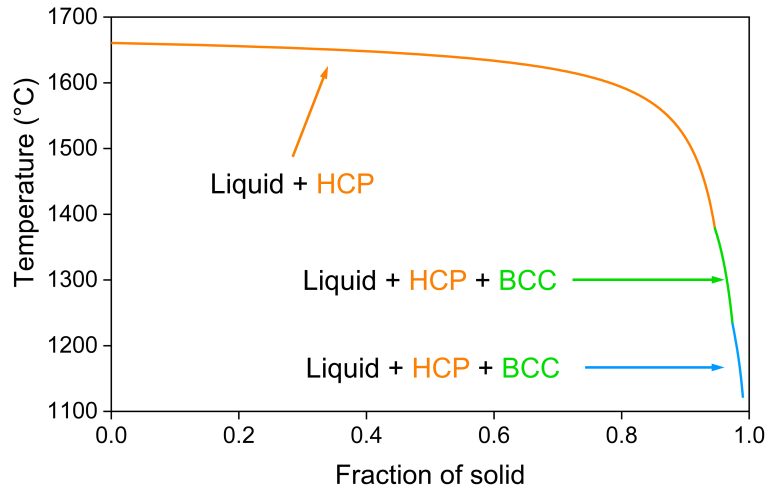
#### **Supplementary Note 4: Experimental validation of simulation layer based on AlCoCrFeNi alloy system**

The chemical composition of the computationally optimized HEAs were close to their experimental compositions (Supplementary Table 5). The tensile test results confirmed the success of AutoMAT's prediction and optimization process of the yield strength (Supplementary Fig. 6). The yield strength increased from 305 MPa to 397 MPa, and the density decreased from 7.33g/cm<sup>3</sup> to 7.17g/cm<sup>3</sup> (Supplementary Table 6).

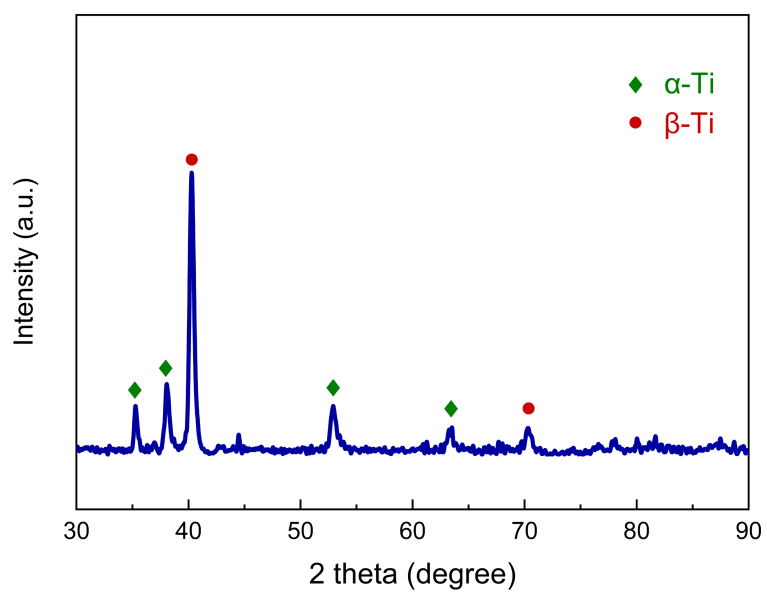
## Supplementary Figures



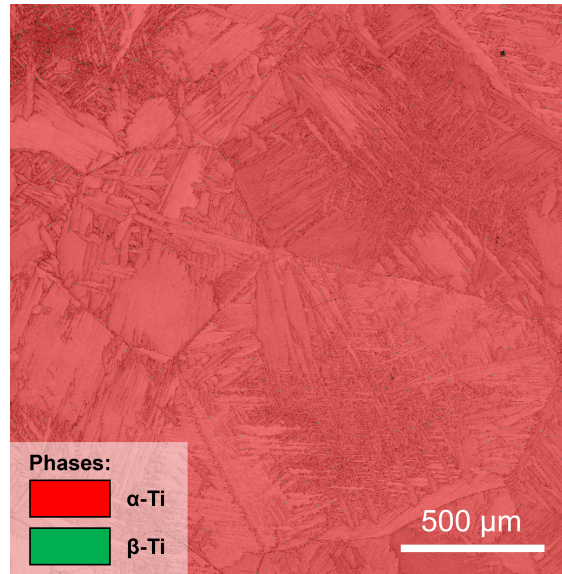
**Supplementary Fig. 1 | Process of using Scheil solidification to improve the reliability of the prediction in the yield strength.**



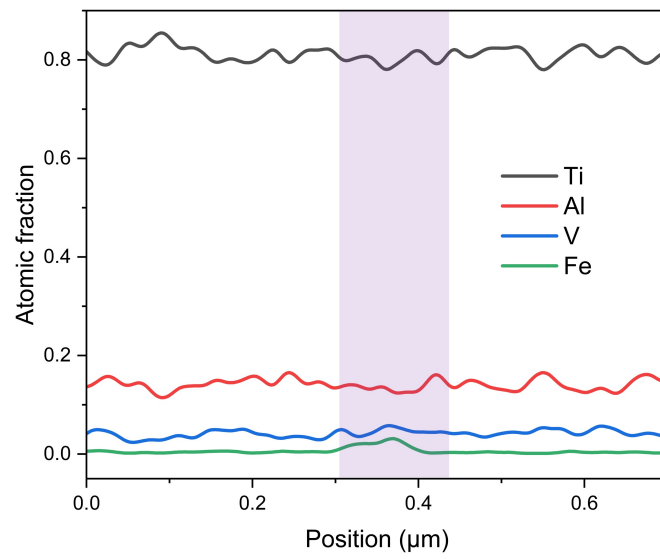
**Supplementary Fig. 2 | Calculated solidification path of the  $\text{Ti}_{81.4}\text{Al}_{16.8}\text{V}_{1.6}\text{Fe}_{0.2}$  alloy by the Scheil model.**



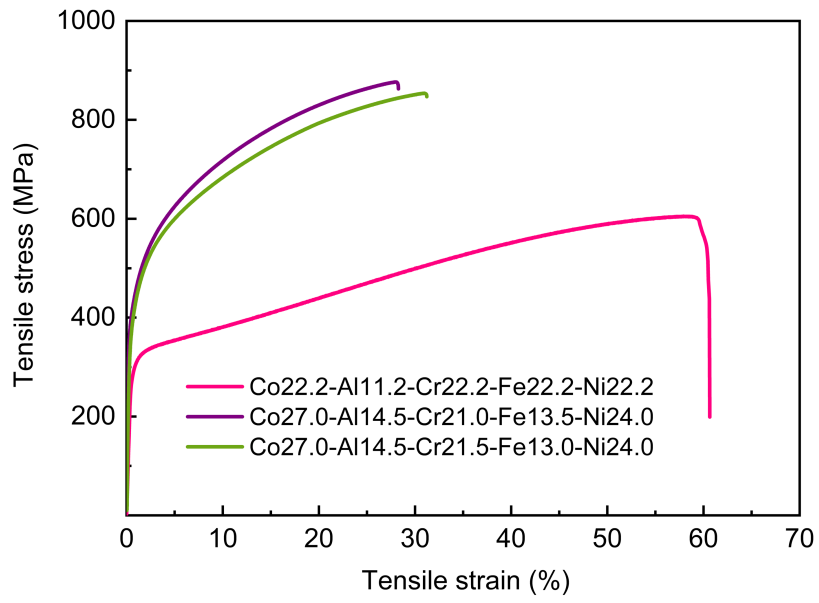
**Supplementary Fig. 3 | XRD pattern of the as-cast Ti<sub>81.4</sub>Al<sub>16.8</sub>V<sub>1.6</sub>Fe<sub>0.2</sub> alloy.**



**Supplementary Fig. 4 | The corresponding EBSD phase map of Fig. 4c.**



**Supplementary Fig. 5 | Compositional profiles recorded across the yellow arrow in Fig. 4d, the purple region indicate the Fe- and V-rich precipitate.**



**Supplementary Fig. 6 | Typical engineering tensile stress-strain curves of the as-cast HEAs.**



## Supplementary Tables

**Supplementary Table 1 | Chemical compositions of the as-cast titanium alloys (in wt%).**

| Alloy                                                                    | Composition  | Ti (%) | Al (%) | V (%) | Fe (%) |
|--------------------------------------------------------------------------|--------------|--------|--------|-------|--------|
| Ti <sub>86.3</sub> Al <sub>1.8</sub> V <sub>7.6</sub> Fe <sub>4.3</sub>  | Nominal      | 86.00  | 1.00   | 8.00  | 5.00   |
|                                                                          | Experimental | 86.09  | 1.08   | 7.93  | 4.90   |
| Ti <sub>82.8</sub> Al <sub>13.0</sub> V <sub>4.0</sub> Fe <sub>0.2</sub> | Nominal      | 87.51  | 7.74   | 4.50  | 0.25   |
|                                                                          | Experimental | 87.62  | 7.67   | 4.44  | 0.27   |
| Ti <sub>81.4</sub> Al <sub>16.8</sub> V <sub>1.6</sub> Fe <sub>0.2</sub> | Nominal      | 87.71  | 10.20  | 1.83  | 0.26   |
|                                                                          | Experimental | 87.30  | 10.61  | 1.82  | 0.27   |

**Supplementary Table 2 | Tensile properties of the as-cast titanium alloys.**

| Alloy                                                                    | Yield strength<br>(MPa) | Ultimate tensile<br>strength (MPa) | Engineering strain<br>(%) |
|--------------------------------------------------------------------------|-------------------------|------------------------------------|---------------------------|
| Ti <sub>86.3</sub> Al <sub>1.8</sub> V <sub>7.6</sub> Fe <sub>4.3</sub>  | 831±6                   | 872±6                              | 7.0±0.3                   |
| Ti <sub>82.8</sub> Al <sub>13.0</sub> V <sub>4.0</sub> Fe <sub>0.2</sub> | 875±23                  | 962±24                             | 4.2±1.0                   |
| Ti <sub>81.4</sub> Al <sub>16.8</sub> V <sub>1.6</sub> Fe <sub>0.2</sub> | 829±14                  | 869±14                             | 2.2±0.6                   |

**Supplementary Table 3 | Theoretical and experimental yield strength of the alloys in Fig. 4b.**

| Alloy                            | Theoretical yield strength (MPa) | Experimental yield strength (MPa) | Reference |
|----------------------------------|----------------------------------|-----------------------------------|-----------|
| Mg-Y11-Al1                       | 92                               | 350                               | [1]       |
| Al-Mg6.0-Sc0.3                   | 63                               | 200                               | [2]       |
| Ti96.63-0.14O-3.23Fe             | 627                              | 744                               | [3]       |
| Ti75.25-Al20-Cr4.75              | N/A                              | 800                               | [4]       |
| Ti82-5Al-5Mo-5V-3Cr              | 540                              | 829.5                             | [5]       |
| Fe41.2-Mn35.2-Co11.8-Cr11.8      | 194                              | 200                               | [6]       |
| Al2.4Co24.4-Cr24.4-Fe24.4-Ni24.4 | 347                              | 185                               | [7]       |
| Nb45-Ta25-Ti15-Hf15              | 484                              | 596                               | [8]       |
| Al19-Fe20-Co20-Ni41              | 442                              | 670                               | [9]       |
| Ti25-Zr25-Hf25-Nb25              | 371                              | 750                               | [10]      |
| Cr20-Mn20-Fe20-Co20-Ni20         | 136                              | 410                               | [11]      |

**Supplementary Table 4 | The EDS chemical compositions of the  $\alpha$  phase and  $\beta$  phase (in at%).**

| Phases   | Ti (%)           | Al (%)           | V (%)           | Fe (%)          |
|----------|------------------|------------------|-----------------|-----------------|
| $\alpha$ | 83.88 $\pm$ 2.30 | 13.97 $\pm$ 1.99 | 1.88 $\pm$ 0.39 | 0.27 $\pm$ 0.07 |
| $\beta$  | 79.81 $\pm$ 2.81 | 12.65 $\pm$ 1.73 | 4.62 $\pm$ 0.88 | 2.92 $\pm$ 0.56 |

**Supplementary Table 5 | Chemical compositions of the as-cast HEAs (in wt%).**

| Alloy                                           | Composition  | Al (%) | Co (%) | Cr (%) | Fe (%) | Ni (%) |
|-------------------------------------------------|--------------|--------|--------|--------|--------|--------|
| $Al_{14.5}Co_{27.0}Cr_{21.5}Fe_{13.0}Ni_{24.0}$ | Nominal      | 7.47   | 30.40  | 21.35  | 13.87  | 26.91  |
|                                                 | Experimental | 7.51   | 30.36  | 21.42  | 13.86  | 26.85  |
| $Al_{14.5}Co_{27.0}Cr_{21.0}Fe_{13.5}Ni_{24.0}$ | Nominal      | 7.47   | 30.38  | 20.85  | 14.40  | 26.90  |
|                                                 | Experimental | 7.48   | 30.33  | 20.88  | 14.39  | 26.92  |

**Supplementary Table 6 | Tensile properties of the as-cast HEAs.**

| Alloy                                                                              | Yield strength (MPa) | Ultimate tensile strength (MPa) | Engineering strain (%) |
|------------------------------------------------------------------------------------|----------------------|---------------------------------|------------------------|
| $\text{Al}_{11.2}\text{Co}_{22.2}\text{Cr}_{22.2}\text{Fe}_{22.2}\text{Ni}_{22.2}$ | 305±9                | 618±13                          | 56.2±5.1               |
| $\text{Al}_{14.5}\text{Co}_{27.0}\text{Cr}_{21.5}\text{Fe}_{13.0}\text{Ni}_{24.0}$ | 378±10               | 854±24                          | 25.2±6.0               |
| $\text{Al}_{14.5}\text{Co}_{27.0}\text{Cr}_{21.0}\text{Fe}_{13.5}\text{Ni}_{24.0}$ | 397±6                | 857±20                          | 26.0±2.3               |

## Supplementary References

1. Zhu, Q. *et al.* Towards development of a high-strength stainless Mg alloy with Al-assisted growth of passive film. *Nat. Commun.* **13**, 5838 (2022).
2. Jiang, S. *et al.* Structurally complex phase engineering enables hydrogen-tolerant Al alloys. *Nature* **641**, 358–364 (2025).
3. Song, T. *et al.* Strong and ductile titanium–oxygen–iron alloys by additive manufacturing. *Nature* **618**, 63–68 (2023).
4. Song, Y. *et al.* A lightweight shape-memory alloy with superior temperature-fluctuation resistance. *Nature* **638**, 965–971 (2025).
5. Zhang, J. *et al.* Ultrauniform, strong, and ductile 3D-printed titanium alloy through bifunctional alloy design. *Science* **383**, 639–645 (2024).
6. Li, Z., Pradeep, K. G., Deng, Y., Raabe, D. & Tasan, C. C. Metastable high-entropy dual-phase alloys overcome the strength–ductility trade-off. *Nature* **534**, 227–230 (2016).
7. Pan, Q. *et al.* Gradient cell–structured high-entropy alloy with exceptional strength and ductility. *Science* **374**, 984–989 (2021).
8. Cook, D. H. *et al.* Kink bands promote exceptional fracture resistance in a NbTaTiHf refractory medium-entropy alloy. *Science* **384**, 178–184 (2024).
9. Shi, P. *et al.* Hierarchical crack buffering triples ductility in eutectic herringbone high-entropy alloys. *Science* **373**, 912–918 (2021).
10. Lei, Z. *et al.* Enhanced strength and ductility in a high-entropy alloy via ordered oxygen complexes. *Nature* **563**, 546–550 (2018).
11. Gludovatz, B. *et al.* A fracture-resistant high-entropy alloy for cryogenic applications. *Science* **345**, 1153–1158 (2014).